

1 **Digital PCR-based deep quantitative profiling delineates** 2 **heterogeneity and evolution of uveal melanoma**

3 R.J. Nell¹
4 M. Versluis¹
5 N.V. Menger¹
6 R.M. Verdijk^{2,3}
7 W.G.M. Kroes⁴
8 H.W. Kapiteijn⁵
9 G.P.M. Luyten¹
10 M.J. Jager¹
11 P.A. van der Velden^{1*}

12

13 ¹ Department of Ophthalmology, Leiden University Medical Center, Leiden, the Netherlands.

14 ² Department of Pathology, Leiden University Medical Center, Leiden, the Netherlands.

15 ³ Department of Pathology, Erasmus MC University Medical Center, Rotterdam, the
16 Netherlands.

17 ⁴ Department of Clinical Genetics, Leiden University Medical Center, Leiden, the
18 Netherlands.

19 ⁵ Department of Medical Oncology, Leiden University Medical Center, Leiden, the
20 Netherlands.

21

22 * Corresponding author, Department of Ophthalmology, Leiden University Medical Center,
23 PO Box 9600, 2300 RC Leiden, The Netherlands

24

25

26 **Acknowledgements**

27 This study was supported by the European Union's Horizon 2020 research and innovation
28 program under grant agreement number 667787 (UM Cure 2020, R.J. Nell and N.V.
29 Menger). We thank D. Cats, H. Mei, L. van Vught and M.C. Gelmi for their help with the
30 sequencing data and clinical information from the patients in this study.

31 **Abstract**

32 Uveal melanoma is an aggressive intraocular tumour characterised by a limited number of
33 genetic alterations. However, the evolution of this malignancy remains enigmatic. In this
34 study, we performed a deep quantitative analysis of 80 primary uveal melanomas by novel
35 digital PCR-based approaches. Mutations were quantified by targeted and drop-off mutation
36 assays, copy number alterations were precisely measured by quantifying the allelic
37 imbalance of heterozygous single-nucleotide polymorphisms. By comparing the absolute
38 abundances of genetic alterations present in a bulk tumour, the heterogeneity and early
39 evolution could be inferred. Tumour progression was further studied by analysing matched
40 primary and metastatic lesions from five patients.

41
42 $G\alpha_q$ signalling mutations were generically and always clonally present, suggesting to be
43 acquired in the earliest stage of uveal melanoma development ('primary driver'). Next, three
44 main evolutionary subtypes could be identified based on having an *EIF1AX* mutation, *SF3B1*
45 mutation or monosomy 3p. These alterations were usually mutually-exclusive and (near-)
46 clonally abundant, suggesting to represent distinct secondary drivers. This contrasts with
47 gains and amplifications of chromosome 8q, which were not restricted to one of the main
48 subtypes and showed subclonality in 31% of the affected tumours. These tertiary alterations
49 were not required for metastatic dissemination.

50
51 Using high-resolution analyses, we identified systematic differences in the evolutionary
52 timing of genetic events in uveal melanoma. The observed intratumour heterogeneity
53 suggests a more complex model of gradual tumour evolution and argues for a
54 comprehensive genetic analysis in clinical practice, which may be facilitated by the sensitive
55 digital PCR assays developed in this study.

56 Introduction

57 Uveal melanoma (UM) is a rare, but often lethal tumour originating from malignantly
58 transformed melanocytes in the choroid, ciliary body or iris in the eye [1, 2]. Unlike other
59 types of melanomas, UMs present with a limited mutational burden and low number of
60 structural variants [3, 4]. Nearly all tumours have a mutation in *GNAQ*, *GNA11*, *PLCB4* or
61 *CYSLTR2*, which activates the $G\alpha_q$ signalling pathway [5-8]. Most melanomas also harbour a
62 so-called BSE mutation in *BAP1*, *SF3B1* or *EIF1AX* [3, 9-11]. The loss of chromosome 3p
63 and the gain (i.e. one extra copy) or amplification (i.e. two or more extra copies) of
64 chromosome 8q are the most prevalent copy number alterations (CNAs), and occur in typical
65 combinations with the BSE mutations [12]. These distinct molecular subtypes are associated
66 with specific gene expression profiles and are differentially correlated with the risk of
67 metastatic spreading and patient survival [12-14].

68
69 Despite the large number of tumours studied, the evolution of UM remains incompletely
70 understood [15-17]. Based on comprehensive bioinformatic analyses, UM has been
71 proposed to arise after an early punctuated burst of the canonical genetic alterations, leading
72 to relatively homogeneous tumours (i.e. most alterations are present in all malignant cells)
73 [15, 17]. However, as most genomic data on UM have been generated by DNA sequencing
74 of low to moderate depths, and the number of mutations is minimal in most tumours, these
75 datasets may lack the power to reliably infer subclonal structures of heterogeneous tumours
76 (i.e. alterations are present in varying proportions of the malignant cells) [18]. Recent work
77 studying UMs in higher resolution (i.e. analyses at the level of single cells or of distinct
78 progression stages) revealed a larger genomic complexity than appreciated previously [16,
79 19]. Though, these studies were carried out in relatively small cohorts or focussed
80 specifically on the evolution of metastatic tumours, leaving the early evolution of primary UM
81 relatively understudied. Moreover, as they were performed using advanced technical
82 approaches, routine application of these techniques remains unavailable in research or
83 clinical diagnostics.

84
85 As an alternative approach, a deep quantitative profiling of individual bulk DNA samples may
86 provide insights into the heterogeneity and evolution of tumours, as we previously
87 demonstrated in familial melanoma and *CYSLTR2* mutant UM [20, 21]. By determining the
88 exact abundance of mutations and CNAs present in the bulk of a tumour, the inferred
89 clonality of these alterations can be used to reconstruct the tumour's genetic history: those
90 alterations that are present in all malignant cells ('clonal') occurred early during tumour

91 evolution, while events present in a subpopulation of the cells ('subclonal') occurred later
92 during progression of the tumour.

93

94 In this study, we perform such in-depth characterisation of 80 primary UMs and five matched
95 metastatic lesions using innovative digital PCR-based assays targeting the key genetic
96 alterations of this malignancy. Hereby, we aim to delineate the heterogeneity of tumours and
97 infer trends in the early and late evolution of UM.

98 **Materials and methods**

99 **LUMC cohort sample collection and DNA/RNA isolation**

100 Primary tumour specimens from 80 fresh-frozen UMs were collected from the biobank of the
101 Department of Ophthalmology, Leiden University Medical Center (LUMC). All samples were
102 obtained from patients primarily treated by enucleation between 2001 and 2011 in the
103 LUMC. In addition, we collected five formalin-fixed and paraffin embedded (FFPE) biopsy
104 specimens from tumour-matched metastatic lesions. This study was approved by the LUMC
105 Biobank Committee and Medisch Ethische Toetsingscommissie under no. B14.003/DH/sh
106 and B20.026. An overview of the clinical characteristics of all cases analysed in this study is
107 presented in **Supplementary Table 1**.

108

109 DNA and RNA were isolated from 25x 20 µm sections using the QIAamp DNA Mini Kit and
110 RNeasy Mini Kit respectively (Qiagen, Hilden, Germany). Total nucleic acid from FFPE
111 tissue was isolated 4x 10 µm macrodissected sections using the Siemens Tissue
112 Preparation System (Siemens Healthcare, Erlangen, Germany) [22]. For all procedures, the
113 manufacturer's instructions were followed.

114

115 **RNA sequencing analysis**

116 We sequenced and analysed 100 ng of RNA per primary tumour sample as described
117 previously [23]. In summary, samples were prepared using the NEBNext Ultra Directional
118 RNA Library Prep Kit for Illumina (New England Biolabs, Ipswich, USA) and sequencing was
119 performed using the Illumina HiSeq 4000 (Illumina, San Diego, USA) by GenomeScan
120 (Leiden, the Netherlands). HiSeq control and image analysis, base calling and quality check
121 were carried out using HCS (version 3.4.0), the Illumina data analysis pipeline RTA (version
122 2.7.7) and Bcl2fastq (version 2.17). Reads were aligned using STAR (version 2.5.3a) to
123 human reference genome GRCh38. Gene counts were generated with htseq-count (version
124 0.6.0) and annotated using Ensembl (version 87). DESeq2 (version 1.30.0) was used for
125 variance stabilising transformation of the count data. All aligned RNA sequencing files were
126 screened for (hotspot) mutations in *GNAQ* (p.Q209, p.R183 and p.G48), *GNA11* (p.Q209,
127 p.R183), *CYSLTR2* (p.L129), *PLCB4* (p.D630), *EIF1AX* (entire gene), *SF3B1* (exon 14) and
128 *BAP1* (entire gene) using freebayes (version 1.3.6), and via manual inspection using the
129 Integrative Genomics Viewer (version 2.8.10). The aligned RNA sequencing files were
130 further analysed for single-nucleotide polymorphisms (SNPs) using VarScan (version 2.3),
131 which were annotated using snpEff/snpSift (version 5.1) according to dbSNP (version 151).
132 Only heterozygously and highly expressed common variants (flagged as 'common', total

133 number of reads > 40, number of reference reads > 2, number of alternate reads > 2) were
134 included in the downstream analysis to identify CNA-derived allelic imbalances.

135

136 **Digital PCR experiments and integration of results**

137 Digital PCR experiments were carried out using the QX200 Droplet Digital PCR System (Bio-
138 Rad Laboratories, Hercules, USA) following the protocols and general guidelines described
139 and discussed earlier [21, 24-27]. In general, 20 ng DNA was analysed in a 22 μ L
140 experiment, using 11 μ L ddPCR™ Supermix for Probes (No dUTP, Bio-Rad) and primers
141 and probes in final concentrations of 900 and 250 nM for duplex experiments, or optimised
142 concentrations for multiplex experiments. The context sequence, PCR annealing
143 temperature and supplier information for all assays used is provided in **Supplementary**
144 **Table 2**.

145

146 PCR mixtures were partitioned into 20.000 droplets using the AutoDG System (Bio-Rad).
147 The PCR was performed in a T100 Thermal Cycler (Bio-Rad) with the following protocol: 10
148 min at 95 °C; 30 s at 94 °C and 1 min at 55 °C, 58 °C or 60 °C (depending on the assay, see
149 **Supplementary Table 2**) for 40 cycles; 10 min at 98 °C; cooling at 12 °C for up to 48 h, until
150 droplet reading. The ramp rate was set to 2 °C/s for all steps. A QX200 Droplet Reader (Bio-
151 Rad) was used to perform reading of the droplets.

152

153 Raw digital PCR results were acquired using QuantaSoft (version 1.7.4, Bio-Rad) and
154 imported and analysed in the online digital PCR management and analysis application
155 Roodcom WebAnalysis (version 2.0, available via <https://webanalysis.roodcom.nl>).

156

157 The $G\alpha_q$ signalling mutations (in *GNAQ*, *GNA11*, *CYSLTR2* and *PLCB4*) and BSE mutations
158 (in *BAP1*, *SF3B1* and *EIF1AX*) were analysed in duplex digital PCR experiments and the
159 measured concentrations (listed between square brackets) of the mutant and wild-type
160 alleles were used to calculate the mutant allele fractions:

161

$$162 \quad \text{mutant allele fraction} = \frac{[\text{mutation}]}{[\text{mutation}] + [\text{wildtype}]}$$

163

164 These values were then used to estimate the mutant cell fractions under heterozygous
165 conditions:

166

$$167 \quad \text{mutant cell fraction} = 2 \cdot \text{mutant allele fraction}$$

168

169 In line with our recent study [27], two approaches were employed to measure CNAs. Firstly,
170 following the classic approach, copy number values were calculated based on the measured
171 concentrations of a DNA target and one stable diploid reference gene:

172

$$173 \quad \text{copy number value} = 2 \cdot \frac{[\text{target}]}{[\text{reference}]}$$

174

175 The targets included genes on chromosome 3p (*PPARG*) and 8q (*PTK2*). Genes on
176 chromosome 5p (*TERT*), 7p (*VOPP1*), 7q (*BRAF*) or 14q (*TTC5*) were evaluated as stable
177 references. Moreover, we used this approach to evaluate the copy number values of the
178 mutant and wild-type alleles in the case of an allelic imbalance affecting the $G\alpha_q$ signalling
179 and BSE genes. As described earlier [21], these additional measurements allowed to
180 calculate the mutant cell fractions under non-heterozygous conditions:

181

$$182 \quad \text{mutant cell fraction (with loss or gain of wild-type allele)} = 2 \cdot \frac{[\text{mutation}]}{[\text{reference}]}$$
$$183 \quad = \text{copy number value} \cdot \text{mutant allele fraction}$$

184

$$185 \quad \text{mutant cell fraction (with gain of mutant allele)} = 2 - 2 \cdot \frac{[\text{wildtype}]}{[\text{reference}]}$$
$$186 \quad = 2 - \text{copy number value} \cdot (1 - \text{mutant allele fraction})$$

187

188 Secondly, following the SNP-based approach, copy number values were measured using
189 the concentrations of haploid genomic loci var_1 and var_2 , representing the two variants of a
190 heterozygous SNP:

191

$$192 \quad \text{copy number value} = 1 + \frac{[\text{var}_1]}{[\text{var}_2]}$$

193

194 In this formula, the SNP variant in the denominator (var_2) is the one assumed to be unaltered
195 and copy number stable (i.e. haploid). When measuring (potential) chromosomal losses, the
196 variant with the highest concentration was chosen as stable variant. Vice versa, the variant
197 with the lowest concentration was assumed to be stable when analysing chromosomal gains
198 and amplifications. Analysed SNPs in this study included rs6617, rs6976, rs9586,
199 rs1989839, rs1062633 and rs2236947 on chromosome 3p, and rs7018178 and rs7843014
200 on chromosome 8q.

201

202 The clonality of the genetic alterations was primarily assessed by comparing the mutant cell
203 fractions in individual tumours. In most samples, the $G\alpha_q$ signalling mutation represented the
204 largest and thus clonal fraction of cancer cells and was considered an accurate estimate of
205 the total fraction malignant cells (i.e. tumour purity). The clonality of CNAs was determined
206 by adjusting the measured copy number values for this tumour purity (assuming that
207 admixed non-malignant cells always have a copy number value of 2). Non-integral outcomes
208 were considered subclonal. For simple CNAs (between -1 and +1), the quantified loss or
209 gain can be mathematically attributed to a specific proportion of the cells in a tumour [21]:

210

211 cell fraction with copy number loss = (2 - copy number value)

212

213 cell fraction with copy number gain = (copy number value - 2)

214

215 For all digital PCR experiments, 99%-confidence intervals were calculated following Fieller's
216 theorem and taken into account in all calculations [28]. *P* values < 0.01 were considered
217 statistically significant.

218

219 **Validation of findings with karyotyping and BAP1 immunohistochemistry**

220 In a selection of cases, the heterogeneity of CNAs and presence and pathogenicity of *BAP1*
221 alterations were confirmed by karyotyping and an immunohistochemical staining, both
222 performed as routine diagnostic analyses in two ISO accredited laboratories (Departments of
223 Pathology, LUMC) [25, 29, 30].

224

225 **Bioinformatic analyses and data availability**

226 The bioinformatic analyses were carried out using R (version 4.0.3) and RStudio (version
227 1.4.1103). Custom scripts and unprocessed results are available via
228 <https://github.com/rjnell/um-heterogeneity>. The molecular interpretation of all cases analysed
229 in this study is presented in **Supplementary Table 1**.

230 Results

231 Sample collection and RNA sequencing analysis

232 Primary UM specimens from 80 patients were studied for mutations and CNAs at the DNA
233 level using digital PCR. As this is a largely targeted technique, RNA sequencing was
234 performed to screen for the presence of genetic alterations, an approach we recently
235 validated for UM [23]. In addition, RNA sequencing was used to divide our cohort into class I
236 (n=29) or class II (n=51) tumours, based on their bulk gene expression profile (GEP). An
237 overview of the molecular and clinical characteristics of all cases is presented in **Figure 1**
238 **and Supplementary Table 1**.

239

240 $G\alpha_q$ and BSE mutation analysis

241 $G\alpha_q$ signalling mutations were detected in 79/80 (99%) tumours of the LUMC cohort and
242 analysed at the DNA level via accustomed targeted digital PCR assays (**Figure 2A and**
243 **Supplementary Table 1**) Although the mutations recurrently affected the established
244 hotspot positions (p.Q209 and p.R183 in *GNAQ/GNA11*, p.D630 in *PLCB4* and p.L129 in
245 *CYSLTR2*), considerable variation was present at the nucleotide level (**Figure 2B**). The
246 *GNAQ* p.G48L mutation, which seems to represent a rare alternative hotspot [12, 16, 31,
247 32], was identified in one tumour.

248

249 *EIF1AX* mutations are known to affect the two first exons of the gene [11], and were
250 detected using RNA sequencing in 11/80 (14%) cases (**Figure 3A and Supplementary**
251 **Table 1**). To verify these mutations at the DNA level, we developed two drop-off digital PCR
252 assays. These assays were designed to target a polymorphic wild-type sequence using two
253 fluorophore-labelled probes within one PCR amplicon [33]. When wild-type alleles are
254 present, a double-positive signal is measured, while when a mutation is present, one of the
255 two probes 'drops off' and single-positive droplets appear (**Figure 3B**). This way, we were
256 able to confirm and quantify the presence of all 11 mutations using only two generic assays.

257

258 *SF3B1* (Splicing Factor 3B subunit 1A) encodes for a component of the splicing machinery
259 and mutations in this gene result in aberrant splicing [3, 34]. Focussing on the exon 14
260 hotspot region, RNA sequencing identified *SF3B1* mutations in 18/80 (23%) melanomas,
261 with 14 cases affecting the p.R625 position (**Figure 3A and Supplementary Table 1**).
262 *SF3B1*-mutation-associated deregulated splicing was observed in 17/18 mutant cases, while
263 this was not detected in any of the *SF3B1*-wild-type tumours (**Figure 3C**). The only
264 discordant case (LUMC-79) harboured a novel *SF3B1* p.A638S mutation of unknown

265 pathogenic significance. The *SF3B1* mutant allele fractions were quantified at the DNA level
266 in 16 cases using digital PCR assays targeting the p.R625C or p.R625H mutation and a
267 dedicated drop-off assay.

268

269 Inactivating *BAP1* mutations (or deletions) can be found throughout the complete *BAP1*
270 gene, challenging the identification of all of these alterations using conventional sequencing
271 [15, 35]. RNA sequencing of our cohort helped us to identify 43/80 (55%) tumours with
272 various types of probably damaging *BAP1* alterations (**Figure 3A and Supplementary**
273 **Table 1**). In five tumours, the sequencing reads insufficiently covered the entire gene, and
274 no conclusions could be drawn on the presence of any mutation. For a selection of cases, an
275 immunohistochemical BAP1 protein staining confirmed the presence or absence of *BAP1*
276 inactivating alterations (**Figure 3D and Supplementary Table 1**). To analyse the exact
277 abundance and clonality of a variety of *BAP1* mutations, we developed one drop-off and
278 eight targeted digital PCR assays by which 15 tumours from our cohort could be
279 characterised.

280

281 **Allele-specific copy number analysis of chromosome 3p and 8q alterations**

282 Extending our recent proof-of-concept study [27], chromosome 3p and 8q CNAs were
283 analysed using two complementary digital PCR-based approaches. For the classic
284 approach, targets on chromosome 3p and 8q were quantified against a stable reference
285 gene using multiplex digital PCR. As a reference-independent alternative, CNA-derived
286 allelic imbalances were measured by quantifying the two variants of heterozygous common
287 SNPs on chromosome 3p and 8q in duplex digital PCR experiments.

288

289 Generally, both approaches resulted in highly comparable copy number values (Spearman's
290 $\rho = 0.95$, $p < 0.001$, **Figure 4A**). By integrating the values determined with the classic and
291 SNP-based approaches, copy number stability of one allele (i.e. one SNP variant) could be
292 assured in most tumours (**Figure 4B**). This confirms our earlier observation that CNAs
293 affecting chromosomes 3p and 8q usually involve only one of both alleles [27]. In our current
294 cohort, we did not identify cases with isodisomy 3p, which would have been visible as a
295 large allelic imbalance in combination with an absent or limited absolute loss of chromosome
296 3p. Moreover, in 49/55 (89%) of the informative tumours, the chromosome 8q copy number
297 value could be correctly estimated based on the allelic (im)balance, which required genomic
298 stability of at least one of both alleles (i.e. one SNP variant). This indicates that 8q copy
299 number increases, including the larger amplifications, are predominantly derived from the
300 (consecutive) gain of the maternal or paternal allele solely (**Figure 4B**). In six tumours we

301 observed that the amplification originated from gaining both alleles. Since the allele-specific
302 copy numbers were significantly different in all these cases (**Supplementary Figure 1A**),
303 these amplifications are likely the result of separate genetic events. As representatively
304 illustrated by case LUMC-75, for which we integrated our copy number data with the allelic
305 imbalances observed in the RNA sequencing data [23], a multi-chromosomal or genome-
306 wide ploidy change could be excluded, indicating that the amplification was acquired via an
307 8q-specific mechanism (**Supplementary Figure 1B**). In 31 tumours, chromosome 3p and/or
308 8q copy numbers could be determined via multiple heterozygous SNPs, which further
309 validated the technical reproducibility of our assays and SNP-based approach
310 (**Supplementary Figure 1C**). As this approach – in line with our recent study [27] – also led
311 to more precise copy number measurements (**Supplementary Figure 1D**), we focussed on
312 the SNP-based results in downstream evaluation of all copy numbers.

313

314 **Clonality analysis integrating mutations and CNAs**

315 By comparing the absolute abundances of the somatic genetic alterations present in a bulk
316 tumour, the clonality and heterogeneity of individual cases can be inferred [36-39]. For this
317 goal, we integrated the quantified mutant allele fractions with the copy number states of the
318 respective genomic loci (indicating zygosity of the mutations, see **Methods**) to determine the
319 $G\alpha_q$, *EIF1AX*, *SF3B1* and *BAP1* mutant cell fractions (**Figure 5A**). Through adjusting all
320 copy number values for tumour purity (i.e. the fraction malignant cancer cells in a tumour
321 sample), the clonality of the various CNAs could also be assessed (**Figure 5A**). This
322 analysis was based on the assumption that CNAs – when clonally present in all malignant
323 cells – should give an integral copy number: -1 for a loss, +1 for a gain and +2, +3, +4 et
324 cetera for an amplification. When the copy number is significantly different from these
325 integral values, the alteration can only originate from a mixture of subpopulations, as
326 exemplified by comparing our bulk measurements to single-cell karyotyping (**Figure 5B**,
327 complete karyograms are presented in **Supplementary Figure 2**). For simple CNAs
328 (between -1 and +1), the quantified loss or gain can be mathematically attributed to a
329 certain proportion of the tumour cells.

330

331 A total of 79/80 primary UMs of our cohort carried a $G\alpha_q$ signalling mutation, which was
332 always clonally expanded (**Figure 5C-D**). Although the $G\alpha_q$ mutations were typically
333 heterozygous, in 8/79 (10%) tumours an additional CNA altered the absolute or relative
334 dosage of the mutant allele. This involved loss of wild-type *GNAQ* (n=3), loss of wild-type
335 *GNA11* (n=1), gain of mutant *GNAQ* (n=1) and gain of wild-type *GNAQ* (n=1), next to the

336 cases with loss of wild-type *CYSLTR2* (n=1) and gain of mutant *CYSLTR2* (n=1) described
337 previously [21]. These additional alterations were subclonal in 6/8 tumours (**Figure 5E**).

338

339 Mutations in *EIF1AX* were found in 10 melanomas and were clonally present in the entire
340 population of malignant cells in nearly all cases (**Figure 5C**). Only one tumour showed a
341 small but significantly detectable fraction of G α_q mutant malignant cells that were *EIF1AX*
342 wild-type ($p < 0.01$, **Figure 5D**). As *EIF1AX* is located on chromosome X, differences were
343 observed in the abundances of mutant and wild-type alleles between female (n=1,
344 heterozygous mutation) and male patients (n=10, hemizygous mutation), but in none of the
345 tumours additional CNAs involving this gene were identified.

346

347 *SF3B1* mutations were found in 18 tumours, of which 16 could be further analysed and also
348 tended to be clonally present (**Figure 5C**). In only one case a small fraction of *SF3B1* wild-
349 type malignant cells ($p < 0.01$, **Figure 5D**) was measured. No CNAs affecting mutant or wild-
350 type *SF3B1* were identified.

351

352 Loss of chromosome 3p was observed in 52/80 (65%) of the tumours. This monosomy was
353 clonally expanded in most tumours (**Figure 5C**). Two GEP class II tumours presented with a
354 small fraction of disomic malignant cells, of which one was *CYSLTR2* mutant and described
355 in our earlier study [21]. Of the GEP class I tumours, only one showed monosomy, which
356 turned out to be subclonally present in a larger fraction of the malignant cells ($p < 0.01$,
357 **Figure 5D**).

358

359 Pathogenic *BAP1* alterations were detected in 46 tumours (all presenting with monosomy
360 3p) and targeted analysis in a selection of 15 tumours confirmed a clonal inactivation of
361 *BAP1* in 14 cases: both the mutation and the loss of the other chromosome 3p were present
362 in the complete G α_q mutant malignant cell fraction (**Figure 5C**). In one tumour, we observed
363 that the *BAP1* mutation was only present in a subclone ($p < 0.01$), while the monosomy 3p
364 was clonally present in all malignant cells (**Figure 5D**).

365

366 Only 15/80 (19%) tumours of our cohort had a normal copy number of chromosome 8q. In
367 those tumours with a detected gain or amplification, large variation was observed in the
368 absolute numbers of additional copies (**Figure 5A**). In total, subclonal gains were found in 13
369 tumours, clonal gains in 17 tumours, subclonal amplifications in 12 tumours and clonal
370 amplifications in 23 tumours.

371

372

373 **Identification of three main UM subtypes based on clonality and mutual-exclusivity**

374 Taken together, a single clonal $G\alpha_q$ signalling mutation was found in nearly all studied
375 tumours, making it the most generic genetic event in our cohort. Though, most UMs acquired
376 additional alterations (**Figure 5A**). Based on trends in their clonality and mutual-exclusivity,
377 three main subgroups of tumours could be defined by (1) a disomy 3p with an *EIF1AX*
378 mutation (8/80, 10% of our cohort), (2) a disomy 3p with an *SF3B1* mutation (14/80, 18%), or
379 (3) a monosomy 3p (47/80, 59%). As these genetic alterations were all (near-)clonally
380 abundant, it is likely that they occurred early during UM development.

381

382 In contrast, chromosome 8q CNAs were not restricted to one of these three subtypes nor
383 obligately present in all tumours of one subtype. Moreover, these copy number increases
384 frequently showed subclonality (**Figure 5A**). This indicates that – in contrast to the clonal
385 alterations – 8q copy number increases were only present in subpopulations of the
386 malignant cells and were acquired at a later evolutionary time point.

387

388 When the loss of chromosome 3p is accompanied by a mutation in *BAP1*, a complete
389 inactivation of this tumour suppressor gene can be accomplished. Similar to the
390 heterogeneity of chromosome 8q CNAs – *BAP1* alterations were not detected in all
391 monosomic tumours of our cohort, *BAP1* protein expression was not always lost and the
392 *BAP1* mutation was not always clonally expanded (**Figure 3D and 5A**).

393

394 The remaining cases (11/80, 14%) were collectively grouped for their 'alternative' profile of
395 genetic alterations with none (n=1) or two clonal $G\alpha_q$ mutations (n=1), a disomy 3p without
396 any detectable BSE mutation (n=5) or with both a clonal *EIF1AX* and *SF3B1* mutation (n=1),
397 a clonal monosomy 3p with both a clonal *BAP1* and *EIF1AX* mutation (n=1) or a clonal *BAP1*
398 and *SF3B1* mutation (n=1), or a clonal *SF3B1* mutation with a subclonal monosomy 3p
399 (n=1). In these tumours chromosome 8q gains and amplifications were also heterogeneously
400 present.

401

402 Of note, the inferred tumour purity differed substantially between individual tumours (median
403 86%, range 25-100%), with the lowest fractions of malignant cells observed in UMs with loss
404 of chromosome 3p (**Figure 5A and Supplementary Table 1**).

405

406 From a clinical perspective, univariate analyses showed that a larger basal diameter, a lack
407 of *SF3B1* mutation, a loss of chromosome 3p and a higher 8q copy number were related to a
408 worse melanoma-related survival (**Table 1**). Age, gender, tumour prominence and having an

409 *EIF1AX* mutation did not reach statistical significance. In a multivariate analysis, only the
410 largest basal diameter of the tumour and the loss of chromosome 3p remained significantly
411 associated with a poor melanoma-related survival.

412

413 **Analysis of five metastases reveals parallel 8q evolution**

414 To investigate the clonality and heterogeneity of the primary UMs in relation to metastatic
415 progression, we extended our study with the genetic analysis of metastatic lesions from five
416 patients of our cohort.

417

418 Several genetic alterations were shared between the primary tumours and matched
419 metastases (**Figure 6A**). This included $G\alpha_q$ signalling mutations in all patients, *SF3B1*
420 mutations in LUMC-42 and -22, chromosome 3p losses in LUMC-29, -79 and -73, and *BAP1*
421 mutations in LUMC-79 and -73. All these alterations were clonally abundant in both primary
422 tumour and metastasis, suggesting to reside on the trunk of the evolutionary trees (**Figure**
423 **6B**).

424

425 Regarding chromosome 8q, however, large variation was observed between the primary and
426 metastatic lesions (**Figure 6A**). In LUMC-29 and -73 no chromosome 8q copy number
427 increases were detected in the primary tumours, but the metastases presented with a
428 subclonal gain or clonal amplification of this chromosome. In LUMC-42 the primary tumour
429 had a clonal 8q gain, but the metastasis presented with a disomy 8q. In LUMC-22 and -79 a
430 subclonal 8q gain was identified in the primary tumour, but the metastatic lesions harboured
431 a subclonal gain and clonal amplification of the other allele of chromosome 8q (**Figure 6A**
432 **and B**).

433

434 In aggregate, 8q copy number increases encompassed independent evolutionary events that
435 could be placed on separate branches of the evolutionary trees (**Figure 6C**). In all patients,
436 the metastatic clone was most likely derived from primary tumour cells carrying a panel of
437 genetic alterations ($G\alpha_q$ signalling mutation, *SF3B1* mutation, chromosome 3p loss and/or
438 *BAP1* mutation), but a disomy 8q. Additional 8q copies were acquired later, during
439 progression of primary tumour or metastasis (**Figure 6C**).

440 Discussion

441 Cancer develops through the accumulation of somatic genetic alterations over time [40, 41].
442 The evolution of human malignancies, including various forms of melanoma, has been
443 elucidated by comparing the genetic make-up of distinct progression stages of individual
444 tumours [42-45]. In UM, however, tumour material is only scarcely available and
445 histologically distinct precursor lesions next to a melanoma are rarely observed [1].
446 Consequently, the (early) evolution of this malignancy remains incompletely understood [15-
447 17]. As an alternative approach, the evolutionary history of an individual tumour can be
448 inferred by a deep quantitative assessment of the genetic alterations present in the bulk of a
449 single tumour biopsy [36-39]. To better understand the development of UM, we performed
450 such in-depth analysis by focussing on the most common mutations and CNAs in this
451 malignancy. For this goal, we successfully screened RNA sequencing data from 80 primary
452 UMs for their genetic alterations, and effectively applied novel, dedicated digital PCR assays
453 to measure the clonality of these alterations at the DNA level.

454
455 In 99% of the tumours in our cohort, we identified an activating $G\alpha_q$ signalling mutation in
456 *GNAQ*, *GNA11*, *CYSLTR2* or *PLCB4*, confirming their ubiquitous presence in UM (**Figure**
457 **1**). We found (almost completely) mutually-exclusive mutations at all established hotspots,
458 including the rare *GNAQ* p.G48 position (**Figure 2B**). As the $G\alpha_q$ signalling mutations were
459 always clonally present, they were likely acquired in one of the earliest stages of tumour
460 development. The common presence of the same mutations in benign nevi and
461 melanocytosis in the eye – both supposed precursors for UM – supports this hypothesis [21,
462 46, 47]. Consequently, a role in tumour initiation ('primary driver') rather than in malignant
463 progression is postulated. Several studies, nevertheless, question the relation between
464 mutations and activity of the $G\alpha_q$ signalling genes and progression of UM [12, 48]. Additional
465 genetic alterations have been described that elevated the allelic balance at the mutant locus
466 towards the *GNAQ* or *CYSLTR2* mutations [16, 21]. We identified such alterations in 9% of
467 the tumours in our cohort, and also one involving *GNA11*. Their typical presence in only a
468 tumour subclone confirms that these alterations were acquired in a later phase, during
469 progression of the primary tumour.

470
471 In addition to the early $G\alpha_q$ signalling mutation, most UMs acquired additional genetic
472 changes. These occurred in typical combinations and followed a recurring order of events,
473 as summarised in **Figure 7A**. Three main evolutionary UM subtypes could be identified
474 based on having an *EIF1AX* mutation, *SF3B1* mutation or monosomy 3p. These three
475 alterations were usually mutually-exclusive and clonally abundant, suggesting to represent

476 distinct 'secondary drivers'. This finding matches with the paradigm that tumours with an
477 *EIF1AX* mutation, *SF3B1* mutation or monosomy 3p represent distinct molecular entities and
478 is in line with earlier reports of the *EIF1AX* and *SF3B1* mutations typically being clonally
479 abundant [12, 15-17, 19]. However, in contrast to some previous studies [49, 50], we only
480 rarely observed heterogeneity of monosomy 3p within the malignant cell population. We
481 hypothesise that the low tumour purity of this latter subtype, sometimes even lower than
482 50% (**Figure 5A**), might explain why disomic and monosomic cells have frequently been
483 found together.

484

485 In contrast, a complete and fully clonal inactivation of *BAP1* was not found in all tumours with
486 monosomy 3p. This confirms occasional observations in earlier studies [12, 15, 16], and
487 suggests that a somatic mutation in this gene should also be seen as a later evolutionary
488 event. However, as complex *BAP1* alterations can be found throughout the entire gene
489 (**Figure 3A**), not all mutations were quantitatively measured using digital PCR and their
490 clonality could only be analysed in a small subset of the tumours.

491

492 We also found that gains and amplifications of chromosome 8q were not restricted to one of
493 the three UM subtypes and frequently showed subclonality. This strongly indicates that these
494 alterations could be seen as a 'tertiary driver'. Intriguingly, the role and evolutionary timing of
495 chromosome 8q increases has remained largely unclear and controversial until now [15-17,
496 25]. Using purity-corrected digital PCR-based quantifications, we generated copy number
497 measurements of much higher precision than previous studies. Although some tumours
498 demonstrated an apparently clonal gain or amplification, at least 31% of our cohort
499 presented with a mixture of cells with different 8q copy numbers, making it the most common
500 heterogeneous genetic alteration in primary UM. We confirmed the presence of this
501 heterogeneity in a number of cases using single-cell karyotyping and by analysing a
502 selection of tumour-matched metastatic lesions. These findings suggest a much more
503 complex role for chromosome 8q in UM biology than acknowledged previously.

504

505 The progressive ramp-up of 8q copy numbers has been reported as one of the most
506 significant genetic changes observed in the evolution from primary UM to metastasis [16].
507 Our results, first of all, suggest that the acquisition of additional 8q copies is an ongoing
508 process during progression of the primary tumour: after the primary and secondary drivers
509 have clonally expanded, subclones with increasing 8q copy numbers may appear. Of note,
510 this increase is usually allele-specific, as it typically solely involves the (consecutive) gain of
511 the maternal or paternal allele. Though, it is not entirely clear how this 8q increase in the
512 primary tumour relates to the metastatic progression of UM. Higher 8q copy numbers have

513 been repetitively associated with a higher frequency of and a shorter time to the
514 development of metastatic disease [12, 24, 51-53]. These associations hold true in our
515 current cohort of tumours and may indicate that melanoma cells with higher 8q levels
516 metastasise more easily. On the other hand, UMs are typically large once detected,
517 suggesting a relatively long time of tumour evolution before the primary lesion is treated (and
518 analysed). The increasing 8q copy numbers might then be seen as a 'molecular clock' of
519 primary tumour progression, while not necessarily influencing the metastatic potential of the
520 individual cancer cells. In line with this hypothesis, all five metastatic lesions we analysed
521 were supposedly disseminated from a primary tumour clone with disomy 8q. Though, 8q
522 gains or amplifications were present in three of the primary tumours and four of the
523 metastatic lesions, but their allele-specificity and subclonality evidenced that these copy
524 number increases were separate genetic events, occurring independently in the late
525 evolution of both primary and metastatic UM (**Figure 7B**).

526
527 Taken together, but in contrast to earlier studies [15, 17], our findings point toward a model
528 of gradual evolution (**Figure 7**) in which a primary driver (i.e. a $G\alpha_q$ signalling mutation)
529 initiates pre-malignant transformation, but a secondary driver (i.e. a mutation in *EIF1AX*, in
530 *SF3B1*, or the loss of chromosome 3p) is required for complete malignant UM development.
531 Subsequently, recurrent tertiary drivers (i.e. most notably chromosome 8q copy number
532 increases) may contribute to full aggressiveness of the cancer, but are not necessary for
533 metastatic dissemination and frequently show heterogeneity within and between tumour
534 lesions in a UM patient.

535
536 From a clinical perspective, the presence of any heterogeneity would necessitate a
537 comprehensive and detailed analysis when relying on the detection of genetic alterations in
538 determining the prognosis or follow-up of patients. This specifically applies to the exact (and
539 thus purity-corrected) measurement of the 8q copy number, as this number is a vital
540 parameter in an established classification system of primary UMs [51, 53, 54]. We propose
541 that the digital PCR assays introduced in this study may be an accessible solution to
542 facilitate this analysis. Additionally, our mutation and copy number assays have potential
543 application in sensitively measuring genetic UM patient material of lower quantity or quality,
544 such as small solid or liquid biopsies. This is illustrated by the successful analysis of FFPE-
545 derived metastases in this study. As another example, some of the mutation assays have
546 already been used in blood-based screening for circulating tumour DNA [55], and the clinical
547 value of similar applications is increasingly recognised [56].

548

549 Critically, our current study is limited by the sole analysis of primary tumours obtained from
550 enucleated eyes, making our cohort being biased toward larger and possibly more evolved
551 (and more clonal) tumours. We hypothesise that the earliest stages of tumour evolution may
552 be studied by comparable in-depth analyses of smaller UMs. In addition, it would be
553 interesting to investigate more pairs of primary and metastatic UMs to better define the later
554 stages of UM evolution. Our evaluations may be further extended to the analysis of other
555 recurrent or sample-specific genetic alterations present in UM.

556

557 In conclusion, using novel digital PCR-based approaches, we identified systematic
558 differences in the evolutionary timing of the key genetic events in UM. The observed
559 intratumour heterogeneity suggests a more complex model of gradual tumour evolution and
560 argues for a comprehensive genetic analysis in clinical practice, which may be facilitated by
561 the sensitive digital PCR assays developed in this study.

562 **Table**

563 **Table 1**

Variable	Univariate		Multivariate	
	HR	<i>p</i> value	HR	<i>p</i> value
Age	1.001	0.941	0.988	0.397
Gender (male versus female)	0.855	0.652	1.160	0.680
Tumour prominence (mm)	1.019	0.744	0.979	0.742
Tumour largest basal diameter (mm)	1.143	<u>0.022</u>	1.149	<u>0.042</u>
<i>EIF1AX</i> mutation (versus wildtype)	0.185	0.096	0.474	0.526
<i>SF3B1</i> mutation (versus wildtype)	0.324	<u>0.035</u>	0.670	0.607
Chromosome 3p loss (versus disomy)	5.667	<u><0.001</u>	4.325	<u>0.040</u>
Chromosome 8q (purity-corrected copy number)	1.397	<u>0.002</u>	0.968	0.840

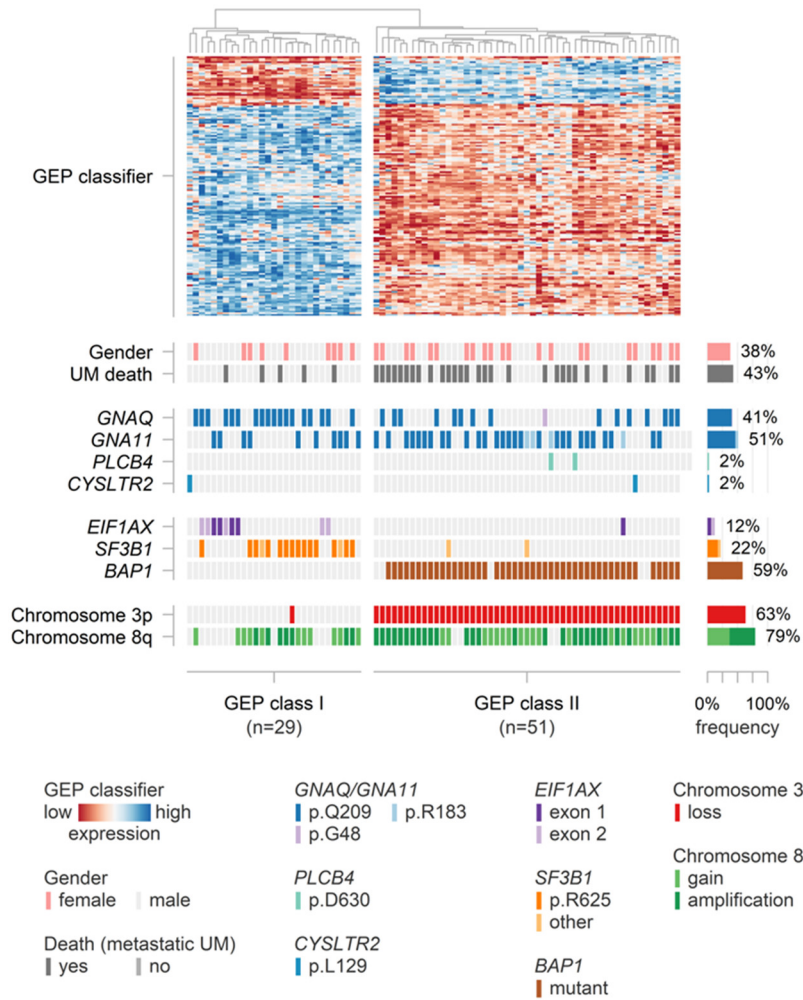
564

565 Uni- and multivariate Cox proportional hazards analysis for factors associated with
566 melanoma-related survival. HR = hazard ratio, vs. = versus, bold underlined *p* values are
567 considered statistically significant (*p* < 0.05).

568

569 **Figures**

570 **Figure 1**



571

572

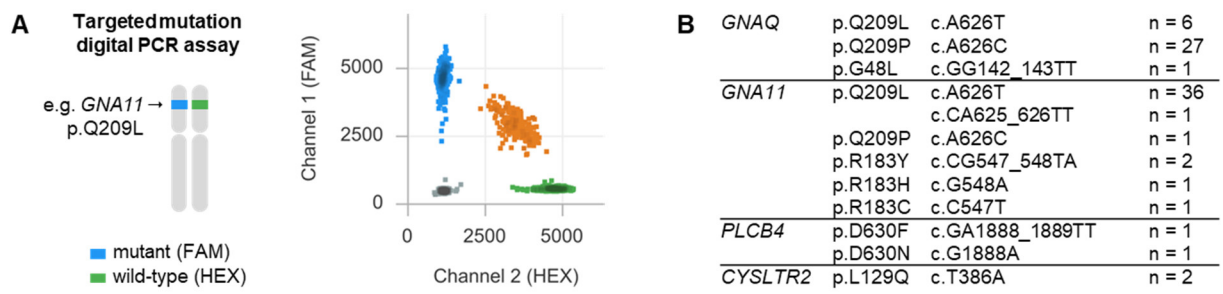
573 Overview of the GEP classification, clinical characteristics and genetic alterations in our

574 LUMC cohort of primary UMs.

575

576

577 **Figure 2**



578

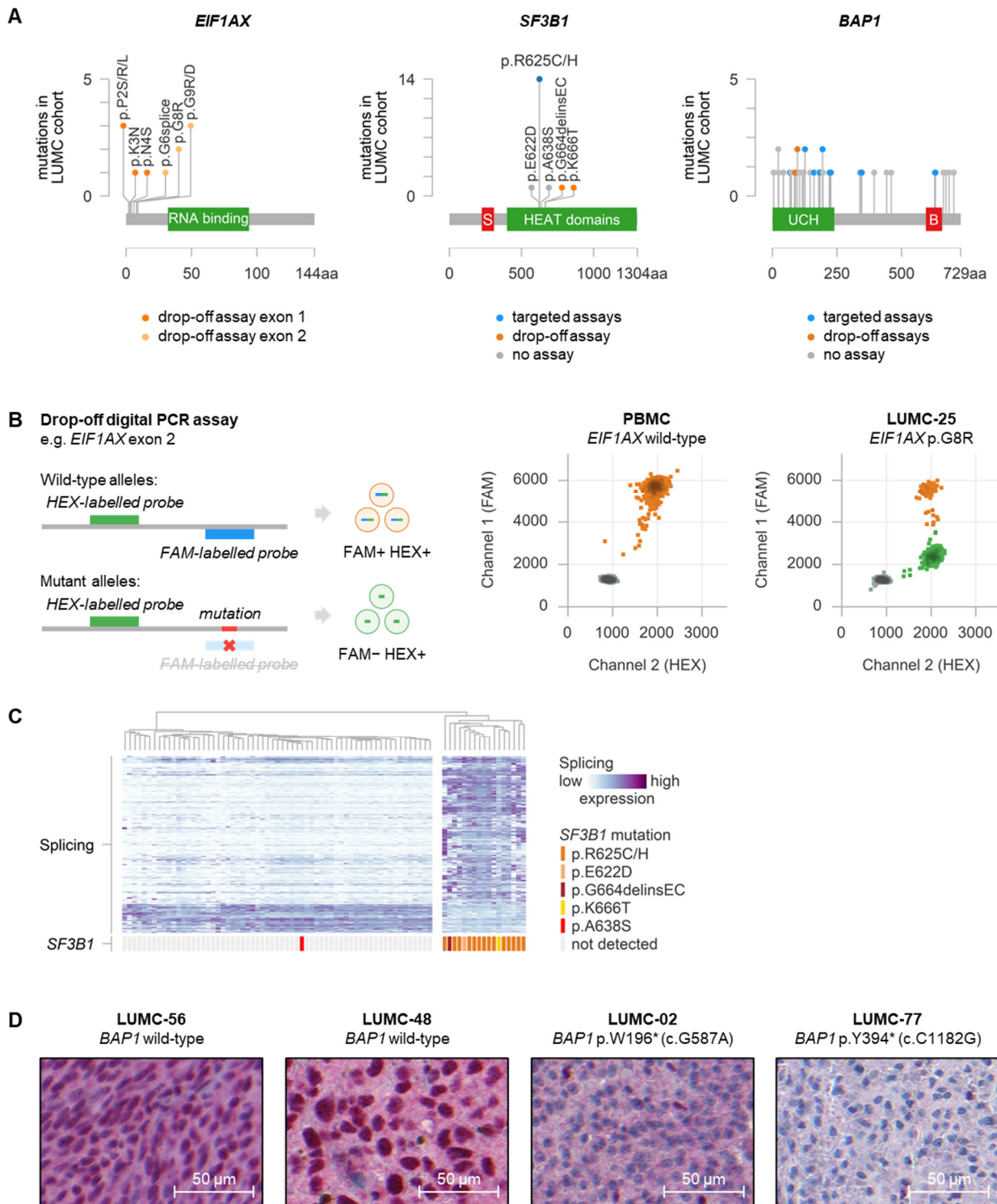
579

580 (A) Analysis of hotspot $G\alpha_q$ signalling mutations using duplex digital PCR with FAM- and
581 HEX-labelled probes targeting the mutant and wild-type sequences.

582 (B) Prevalence and exact nucleotide variation of the $G\alpha_q$ signalling mutations in the LUMC

583 cohort.

584 **Figure 3**



585

586

587 (A) Lollipop plots demonstrating the distribution and prevalence of mutations in *EIF1AX*,
588 *SF3B1* and *BAP1* in the LUMC cohort. The colors refer the digital PCR assays available to
589 analyse these mutations. Red and green boxes refer to selected gene domains.

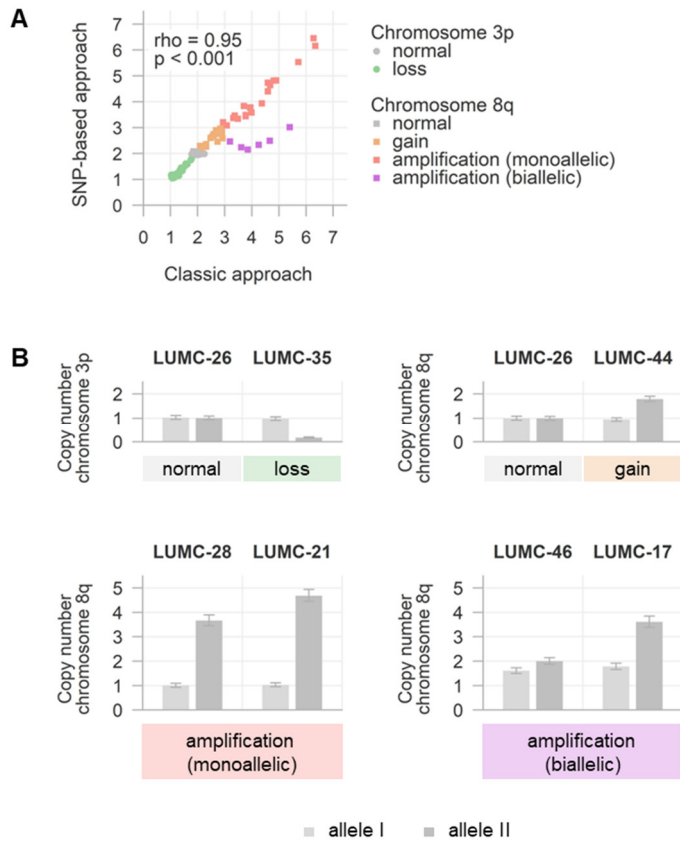
590 (B) Illustration of the principle behind the digital PCR drop-off assays with two 2D plots as
591 examples of the *EIF1AX* exon 2 drop-off analysis.

592 (C) Analysis of a signature of alternative splicing to identify *SF3B1* mutant tumours.

593 (D) Representative immunohistochemical BAP1 nuclear stainings demonstrating preserved
594 staining in *BAP1* wild-type tumours and lost staining in tumours with a *BAP1* mutation.

595

596 **Figure 4**

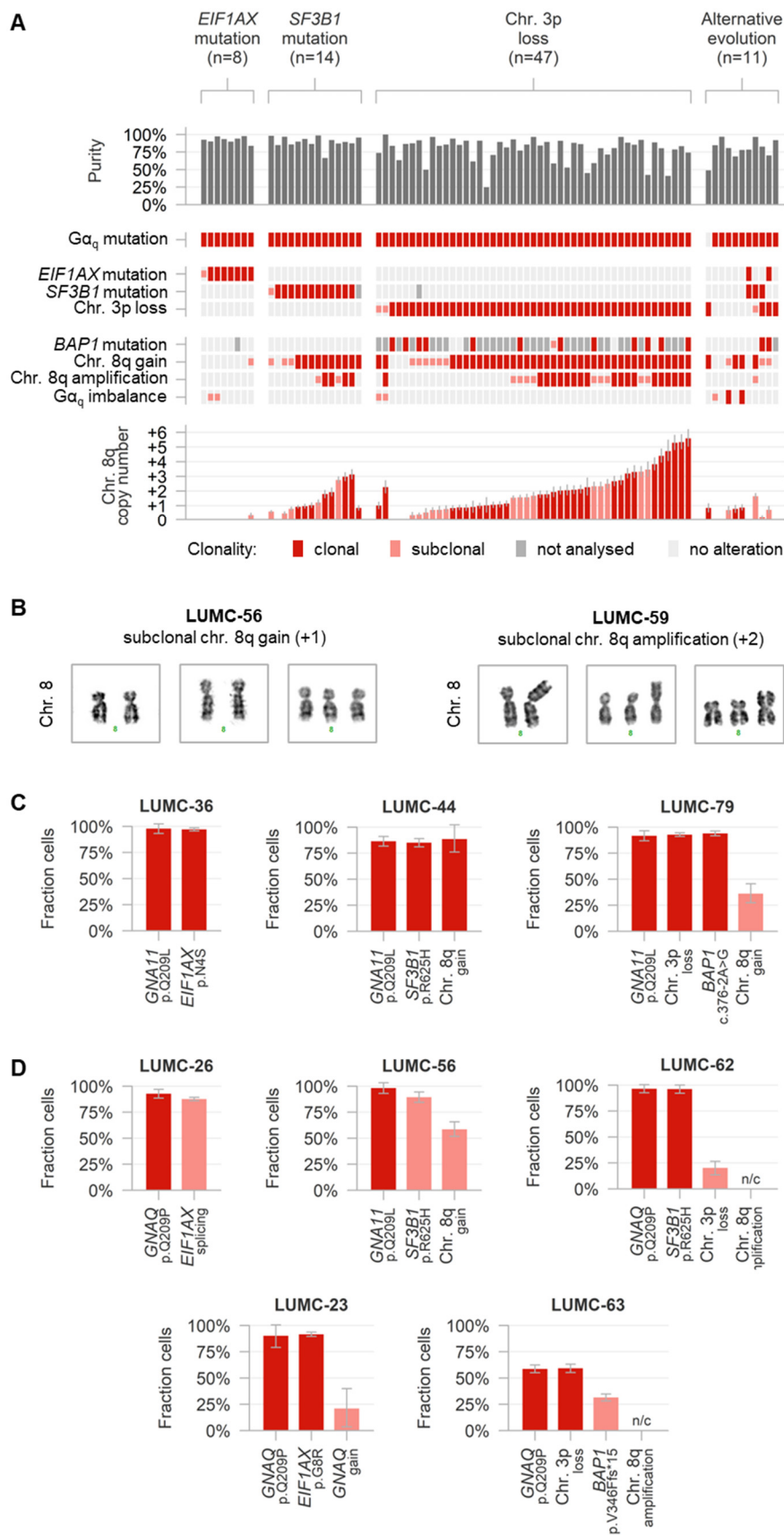


597

598 (A) Comparison of chromosome 3p and 8q copy number values determined with the classic
 599 and SNP-based approaches.

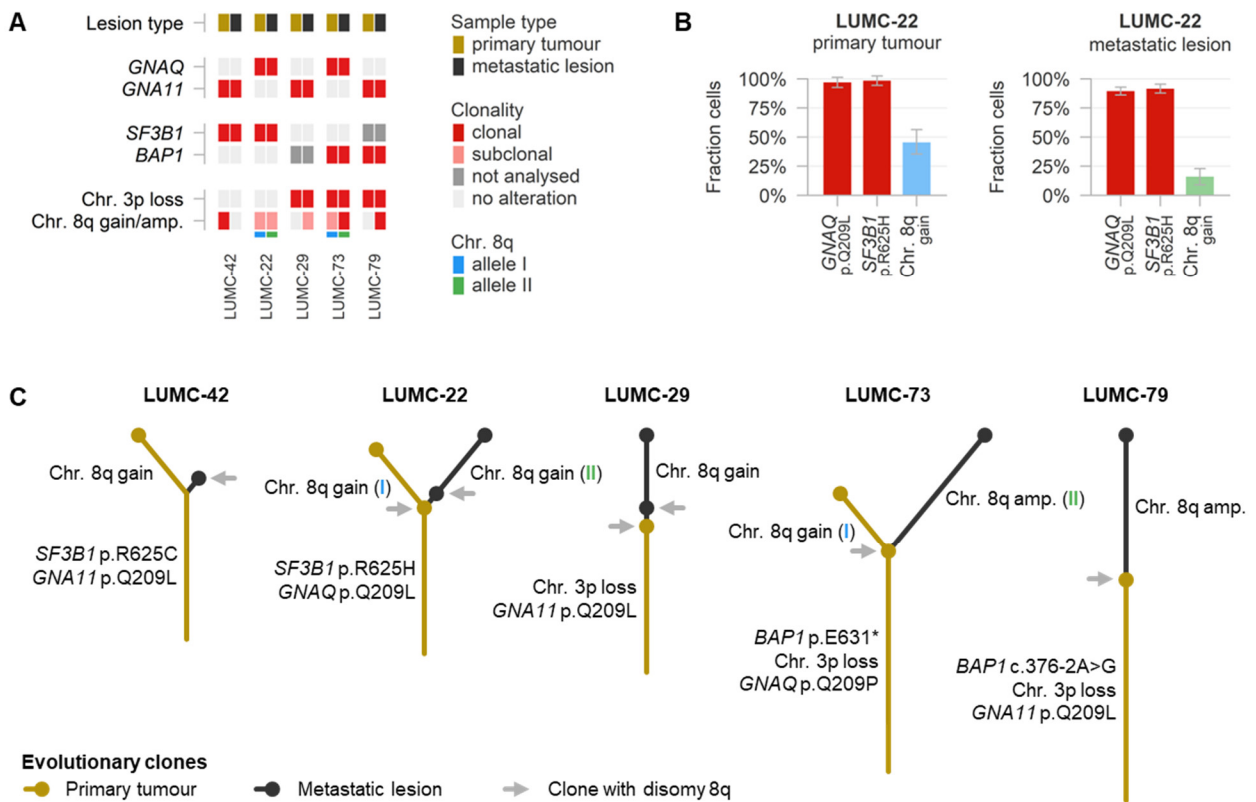
600 (B) Examples of integrated copy number values determined with both approaches, revealing
 601 the allele-specificity behind the various alterations.

602 **Figure 5**



604 **(A)** Overview of presence, clonality and mutual-exclusivity of the various genetic alterations
605 in the LUMC cohort. Additionally, the measured tumour purities and purity-corrected
606 chromosome 8q copy number values are presented
607 **(B)** Evidence of chromosome 8q heterogeneity by single-cell karyotyping.
608 **(C)** Examples of tumours with multiple clonal genetic alterations.
609 **(D)** Examples of tumours with a clonal $G\alpha_q$ signalling mutation and additional (sub)clonal
610 alterations. N/c: not calculable.

611 **Figure 6**



612
613

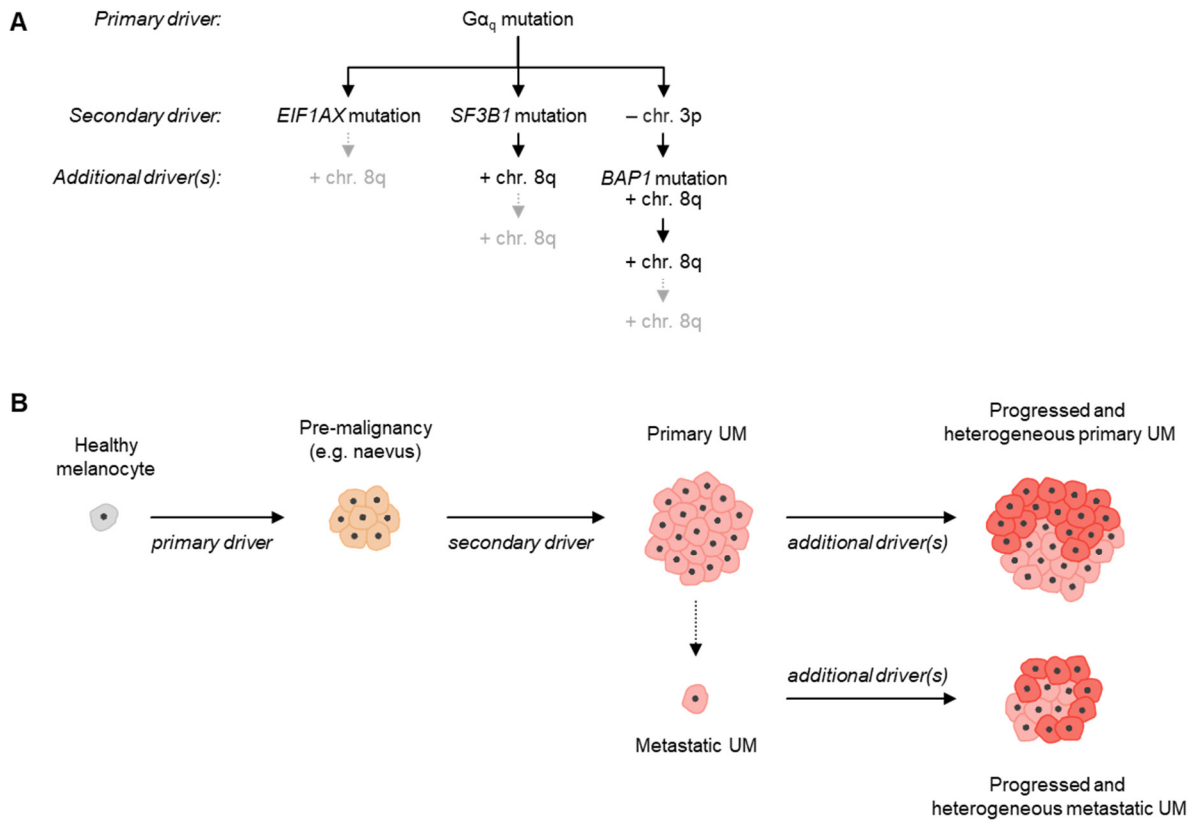
614 **(A)** Overview of genetic alterations and their clonality in five pairs of primary tumours and
615 metastatic lesions. Additionally, the allele-specificity of the chromosome 8q CNAs is
616 presented.

617 **(B)** Extended from **A**. Detailed example of the clonality analysis in the samples from case
618 LUMC-22. Note that the chromosome 8q gain is subclonally present in both samples, but
619 involves a different allele.

620 **(C)** Inferred evolutionary trees of the uveal melanomas from the five patients.

621

622 **Figure 7**



623

624 (A) Main evolutionary subtypes of UMs with specified primary, secondary and additional
625 genetic alterations driving this evolution.

626 (B) Proposed model of gradual tumour evolution ultimately leading to heterogeneous primary
627 and metastatic UMs.

628 References

- 629 1. Coupland, S.E., et al., *Molecular pathology of uveal melanoma*. Eye (Lond), 2013. **27**(2): p.
630 230-42.
- 631 2. Jager, M.J., et al., *Uveal melanoma*. Nat Rev Dis Primers, 2020. **6**(1): p. 24.
- 632 3. Furney, S.J., et al., *SF3B1 mutations are associated with alternative splicing in uveal*
633 *melanoma*. Cancer Discov, 2013. **3**(10): p. 1122-1129.
- 634 4. Royer-Bertrand, B., et al., *Comprehensive Genetic Landscape of Uveal Melanoma by Whole-*
635 *Genome Sequencing*. Am J Hum Genet, 2016. **99**(5): p. 1190-1198.
- 636 5. Van Raamsdonk, C.D., et al., *Frequent somatic mutations of GNAQ in uveal melanoma and*
637 *blue naevi*. Nature, 2009. **457**(7229): p. 599-602.
- 638 6. Van Raamsdonk, C.D., et al., *Mutations in GNA11 in uveal melanoma*. N Engl J Med, 2010.
639 **363**(23): p. 2191-9.
- 640 7. Johansson, P., et al., *Deep sequencing of uveal melanoma identifies a recurrent mutation in*
641 *PLCB4*. Oncotarget, 2016. **7**(4): p. 4624-31.
- 642 8. Moore, A.R., et al., *Recurrent activating mutations of G-protein-coupled receptor CYSLTR2 in*
643 *uveal melanoma*. Nat Genet, 2016. **48**(6): p. 675-80.
- 644 9. Harbour, J.W., et al., *Frequent mutation of BAP1 in metastasizing uveal melanomas*. Science,
645 2010. **330**(6009): p. 1410-3.
- 646 10. Harbour, J.W., et al., *Recurrent mutations at codon 625 of the splicing factor SF3B1 in uveal*
647 *melanoma*. Nat Genet, 2013. **45**(2): p. 133-5.
- 648 11. Martin, M., et al., *Exome sequencing identifies recurrent somatic mutations in EIF1AX and*
649 *SF3B1 in uveal melanoma with disomy 3*. Nat Genet, 2013. **45**(8): p. 933-6.
- 650 12. Robertson, A.G., et al., *Integrative Analysis Identifies Four Molecular and Clinical Subsets in*
651 *Uveal Melanoma*. Cancer Cell, 2017. **32**(2): p. 204-220 e15.
- 652 13. Yavuziyigitoglu, S., et al., *Uveal Melanomas with SF3B1 Mutations: A Distinct Subclass*
653 *Associated with Late-Onset Metastases*. Ophthalmology, 2016. **123**(5): p. 1118-28.
- 654 14. Onken, M.D., et al., *Gene expression profiling in uveal melanoma reveals two molecular*
655 *classes and predicts metastatic death*. Cancer Res, 2004. **64**(20): p. 7205-9.
- 656 15. Field, M.G., et al., *Punctuated evolution of canonical genomic aberrations in uveal melanoma*.
657 Nat Commun, 2018. **9**(1): p. 116.
- 658 16. Shain, A.H., et al., *The genetic evolution of metastatic uveal melanoma*. Nat Genet, 2019.
659 **51**(7): p. 1123-1130.
- 660 17. Rodrigues, M., et al., *Evolutionary Routes in Metastatic Uveal Melanomas Depend on MBD4*
661 *Alterations*. Clin Cancer Res, 2019. **25**(18): p. 5513-5524.
- 662 18. Caravagna, G., et al., *Subclonal reconstruction of tumors by using machine learning and*
663 *population genetics*. Nat Genet, 2020. **52**(9): p. 898-907.
- 664 19. Durante, M.A., et al., *Single-cell analysis reveals new evolutionary complexity in uveal*
665 *melanoma*. Nat Commun, 2020. **11**(1): p. 496.
- 666 20. Christodoulou, E., et al., *Loss of Wild-Type CDKN2A Is an Early Event in the Development of*
667 *Melanoma in FAMMM Syndrome*. J Invest Dermatol, 2020. **140**(11): p. 2298-2301 e3.
- 668 21. Nell, R.J., et al., *Involvement of mutant and wild-type CYSLTR2 in the development and*
669 *progression of uveal nevi and melanoma*. BMC Cancer, 2021. **21**(1): p. 164.
- 670 22. van Eijk, R., et al., *Assessment of a fully automated high-throughput DNA extraction method*
671 *from formalin-fixed, paraffin-embedded tissue for KRAS, and BRAF somatic mutation*
672 *analysis*. Exp Mol Pathol, 2013. **94**(1): p. 121-5.
- 673 23. Nell, R.J., et al., *Identification of clinically-relevant genetic alterations in uveal melanoma*
674 *using RNA sequencing*. 2023.
- 675 24. Versluis, M., et al., *Digital PCR validates 8q dosage as prognostic tool in uveal melanoma*.
676 PLoS One, 2015. **10**(3): p. e0116371.
- 677 25. de Lange, M.J., et al., *Heterogeneity revealed by integrated genomic analysis uncovers a*
678 *molecular switch in malignant uveal melanoma*. Oncotarget, 2015. **6**(35): p. 37824-35.
- 679 26. Zoutman, W.H., R.J. Nell, and P.A. van der Velden, *Usage of Droplet Digital PCR (ddPCR)*
680 *Assays for T Cell Quantification in Cancer*. Methods Mol Biol, 2019. **1884**: p. 1-14.
- 681 27. Nell, R.J., et al., *Allele-specific digital PCR enhances precision and sensitivity in the detection*
682 *and quantification of copy number alterations in heterogeneous DNA samples: an in silico and*
683 *in vitro validation study*. medRxiv, 2023: p. 2023.10.31.23297362.
- 684 28. Dube, S., J. Qin, and R. Ramakrishnan, *Mathematical analysis of copy number variation in a*
685 *DNA sample using digital PCR on a nanofluidic device*. PLoS One, 2008. **3**(8): p. e2876.

- 686 29. Smit, K.N., et al., *Combined mutation and copy-number variation detection by targeted next-*
687 *generation sequencing in uveal melanoma*. *Mod Pathol*, 2018. **31**(5): p. 763-771.
- 688 30. van Essen, T.H., et al., *Prognostic parameters in uveal melanoma and their association with*
689 *BAP1 expression*. *Br J Ophthalmol*, 2014. **98**(12): p. 1738-43.
- 690 31. Johnson, C.P., et al., *Systematic genomic and translational efficiency studies of uveal*
691 *melanoma*. *PLoS One*, 2017. **12**(6): p. e0178189.
- 692 32. Johansson, P.A., et al., *Whole genome landscapes of uveal melanoma show an ultraviolet*
693 *radiation signature in iris tumours*. *Nat Commun*, 2020. **11**(1): p. 2408.
- 694 33. Bidshahri, R., et al., *Quantitative Detection and Resolution of BRAF V600 Status in Colorectal*
695 *Cancer Using Droplet Digital PCR and a Novel Wild-Type Negative Assay*. *J Mol Diagn*, 2016.
696 **18**(2): p. 190-204.
- 697 34. Alsafadi, S., et al., *Cancer-associated SF3B1 mutations affect alternative splicing by*
698 *promoting alternative branchpoint usage*. *Nat Commun*, 2016. **7**: p. 10615.
- 699 35. Karlsson, J., et al., *Molecular profiling of driver events in metastatic uveal melanoma*. *Nat*
700 *Commun*, 2020. **11**(1): p. 1894.
- 701 36. Durinck, S., et al., *Temporal dissection of tumorigenesis in primary cancers*. *Cancer Discov*,
702 2011. **1**(2): p. 137-43.
- 703 37. Nik-Zainal, S., et al., *The life history of 21 breast cancers*. *Cell*, 2012. **149**(5): p. 994-1007.
- 704 38. Mitchell, T.J., et al., *Timing the Landmark Events in the Evolution of Clear Cell Renal Cell*
705 *Cancer: TRACERx Renal*. *Cell*, 2018. **173**(3): p. 611-623 e17.
- 706 39. Gerstung, M., et al., *The evolutionary history of 2,658 cancers*. *Nature*, 2020. **578**(7793): p.
707 122-128.
- 708 40. Martincorena, I. and P.J. Campbell, *Somatic mutation in cancer and normal cells*. *Science*,
709 2015. **349**(6255): p. 1483-9.
- 710 41. Jolly, C. and P. Van Loo, *Timing somatic events in the evolution of cancer*. *Genome Biol*,
711 2018. **19**(1): p. 95.
- 712 42. Gerlinger, M., et al., *Intratumor heterogeneity and branched evolution revealed by multiregion*
713 *sequencing*. *N Engl J Med*, 2012. **366**(10): p. 883-892.
- 714 43. Shain, A.H., et al., *The Genetic Evolution of Melanoma from Precursor Lesions*. *N Engl J*
715 *Med*, 2015. **373**(20): p. 1926-36.
- 716 44. Jamal-Hanjani, M., et al., *Tracking the Evolution of Non-Small-Cell Lung Cancer*. *N Engl J*
717 *Med*, 2017. **376**(22): p. 2109-2121.
- 718 45. Shain, A.H., et al., *Genomic and Transcriptomic Analysis Reveals Incremental Disruption of*
719 *Key Signaling Pathways during Melanoma Evolution*. *Cancer Cell*, 2018. **34**(1): p. 45-55 e4.
- 720 46. Vader, M.J.C., et al., *GNAQ and GNA11 mutations and downstream YAP activation in*
721 *choroidal nevi*. *Br J Cancer*, 2017. **117**(6): p. 884-887.
- 722 47. Durante, M.A., et al., *Genomic evolution of uveal melanoma arising in ocular melanocytosis*.
723 *Cold Spring Harb Mol Case Stud*, 2019. **5**(4).
- 724 48. Silva-Rodriguez, P., et al., *GNAQ and GNA11 Genes: A Comprehensive Review on*
725 *Oncogenesis, Prognosis and Therapeutic Opportunities in Uveal Melanoma*. *Cancers (Basel)*,
726 2022. **14**(13).
- 727 49. Maat, W., et al., *The heterogeneous distribution of monosomy 3 in uveal melanomas:*
728 *implications for prognostication based on fine-needle aspiration biopsies*. *Arch Pathol Lab*
729 *Med*, 2007. **131**(1): p. 91-6.
- 730 50. Mensink, H.W., et al., *Chromosome 3 intratumor heterogeneity in uveal melanoma*. *Invest*
731 *Ophthalmol Vis Sci*, 2009. **50**(2): p. 500-4.
- 732 51. Vichitvejpaisal, P., et al., *Genetic Analysis of Uveal Melanoma in 658 Patients Using the*
733 *Cancer Genome Atlas Classification of Uveal Melanoma as A, B, C, and D*. *Ophthalmology*,
734 2019. **126**(10): p. 1445-1453.
- 735 52. Thornton, S., et al., *Targeted Next-Generation Sequencing of 117 Routine Clinical Samples*
736 *Provides Further Insights into the Molecular Landscape of Uveal Melanoma*. *Cancers (Basel)*,
737 2020. **12**(4).
- 738 53. Shields, C.L., et al., *Ten-year outcomes of uveal melanoma based on The Cancer Genome*
739 *Atlas (TCGA) classification in 1001 cases*. *Indian J Ophthalmol*, 2021. **69**(7): p. 1839-1845.
- 740 54. Jager, M.J., N.J. Brouwer, and B. Esmaeli, *The Cancer Genome Atlas Project: An Integrated*
741 *Molecular View of Uveal Melanoma*. *Ophthalmology*, 2018. **125**(8): p. 1139-1142.
- 742 55. Beasley, A., et al., *Clinical Application of Circulating Tumor Cells and Circulating Tumor DNA*
743 *in Uveal Melanoma*. *JCO Precis Oncol*, 2018. **2**.

- 744 56. Carvajal, R.D., et al., *Clinical and molecular response to tebentafusp in previously treated*
745 *patients with metastatic uveal melanoma: a phase 2 trial*. Nat Med, 2022. **28**(11): p. 2364-
746 2373.
747